SUPPLEMENTARY MATERIALS AND METHODS

1. Cell lines.

Hep3B and PLC/PRF/5 cell lines were obtained from European Collection of Cell Cultures (ECACC, Porton Down, Salisbury, Wiltshire, UK) in 2004 and 2008, respectively. When initiated this study (2014), cell authentication was performed. *In vitro* experiments were finished at the end of 2017. Cell lines were never used in the laboratory for longer than 3 months after receipt or resuscitation.

2. Cell culture on thick layers of collagen I.

Fibrillar bovine collagen I (Ref. 5005; PureCol, Advanced BioMatrix, San Diego, CA, USA) was prepared at 1.7 mg/ml in DMEM according to manufacturer's protocol. After polymerisation (4h-37°C, 10% CO_2), cells were seeded on top in medium containing 10% FBS and allowed to adhere for 24h.

3. Treatments.

Response to TGF-β was analysed adding human recombinant TGF-β1 (2ng/mL) (Ref. 616455, Calbiochem, La Jolla, CA, USA) to the culture (complete medium, 10% FBS) for a total of 72h. For experiments analysing the response to EGF, cells at 60% confluence were serum-starved for 16h and treated with EGF (20ng/mL) (Ref. E9644, Sigma-Aldrich, St. Louis, MO, USA).

4. Knockdown assays.

For stable silencing with short hairpin RNA (shRNA), cells at 50-60% confluence were transfected with MAtra-A reagent (Ref. 7-2001-020, IBA GmbH, Goettingen, Germany), 1:600 in complete medium, according to manufacturer's recommendation (15min on the magnet plate), using 2µg/ml shRNA plasmid. After 24h, medium was changed to complete medium, and selection was done with puromycin (Ref. 58-

58-2, InvivoGen Therapeutics, France) for at least 50 days before experiments. See **Supplementary Table S1** for shRNA sequences. Pools of transfected cells rather than individual clones were selected to avoid potential clone-to-clone variations, and best-silenced pools of transfected cells were selected (from now *clones*). Best-silenced clones were chosen and at least two different clones were used in each cell line. Cell line and clone used are indicated in each figure.

5. Analysis of gene expression.

When RNA was isolated from cells, p60 culture plates were washed with PBS and cells were scrapped in 350µl of a solution containing RLT Buffer (from the Kit) previously adding 10µl/mL of β-Mercaptoethanol. When RNA was isolated from tissues, small pieces of frozen tissues were pulverized mechanically in a mortar (sterilized at 200ºC-4h to inactivate RNAses), then tissue powder was transferred to an eppendorf and resuspended in 600µL of RLT+β-Mercaptoethanol. mRNA levels for each gene were determined following manufacturers' protocols and normalized with a housekeeping gene (*RPL32* for HCC cells and *SFRS4* for human samples from HCC patients). See **Supplementary Table S2** for primers sequences.

6. Western blot analysis.

Cells were lysed in RIPA lysis buffer (0.5% Sodium deoxycholate, 30mM Tris-HCl pH 7.5, 0.1% SDS, 1% Triton-X-100, 150mM NaCl, 5mM EDTA, 10% Glycerol, 1mM PMSF, 5µg/mL Leupeptin, 0.1mM Na_3VO_4, 0.5mM DTT, 20mM β-Glycerolphosphate) for 1h at 4ºC. Antibodies used are summarized in **Supplementary Table S3**. Densitometric analysis of protein intensity was performed using ImageJ software (National Institutes of Health (NIH), Bethesda, MD, USA).

7. Immunofluorescence, confocal microscopy and image quantification.

Epifluorescence microscopy studies were performed as previously described (1). Contrast phase pictures of cells on culture were taken with Olympus 70iX microscope and a Spot 4.3 digital camera and software.

For the immunostaining of cells seeded on gelatin (no-coating) or fibronectin-coated (Ref. 354008, BD Biosciences, Bedford, MA, USA) (1.5μg/cm^2) glass coverslips, cells were fixed with 4% paraformaldehyde for 30 min and immunostained for β-CATENIN, CYTOKERATIN-18, EGFR, phalloidin-TRITC for F-ACTIN detection, VINCULIN or ZO-1; to detect E-CADHERIN and VIMENTIN, cells were fixed with methanol for 2 min. DAPI (Ref. 28718-90-3, Sigma-Aldrich, St. Louis, MO, USA) staining was used to elucidate the number of cells. Primary antibodies and conditions used are detailed in **Supplementary Table S3**. Secondary antibodies Alexa Fluor 488-conjugated anti-rabbit and anti-mouse immunoglobulin were from Molecular Probes (Eugene, OR, USA). Cells were visualized in a Nikon eclipse 80i microscope with appropriate filters. Representative images were taken with a Nikon DS-Ri1 digital camera using NIS-Elements BR 3.2 (64-bit) software. VINCULIN with F-ACTIN staining (for focal adhesions studies) was visualized on a Leica TCS SP5 spectral confocal microscope with a HCX PL APO λ blue 40x 1.4 oil objective lens. Acquisition software was LEICA application suite advanced fluorescence (LAS AF). Confocal Z-slice images were analysed using ImageJ software.

For the immunostaining of cells seeded on top of a thick collagen I matrix, cells were fixed with 12% paraformaldehyde and immunostained for pMLC2 and phalloidin-TRITC for F-ACTIN detection as described (2). For the imaging, collagen gels with immunostained cells were transferred to glass-bottomed dishes and visualized on a Leica TCS SP5 spectral confocal microscope (as described above). pMLC2 fluorescence signal was quantified calculating the pixel intensity in single cell/group relative to the cell area (determined using F-ACTIN staining) and cell number (determined using DRAQ5 - Ref. DR05500, Biostatus, UK – staining), using ImageJ software. Representative images were edited in Adobe Photoshop software.

8. Adhesion assay.

Real-time cell adhesion was examined using the xCELLigence System (ACEA Biosciences, Inc., San Diego, CA, USA) (2). Overall, 1.25×10^4 cells/well (final volume of 100µL) were seeded onto an E-plate 16 (Ref. 05469830001, ACEA Biosciences, Inc., San Diego, CA, USA), which features microelectronic sensors integrated on the bottom of the plate. To analyse cell adhesion to different extracellular matrix, wells were previously coated during 30 min with fibronectin (Ref. 354008, BD Biosciences, Bedford, MA, USA) (1.5µg/cm^2) or non-coated. Continuous values were represented as cell index (CI), a dimensionless parameter reflecting a relative change in measured electrical impedance, and quantified as a slope (*per* hour) of the first 3h.

9. Migration assays.

Cell motility was examined by: (i) real-time migration assay through the xCELLigence System (ACEA Biosciences, Inc., San Diego, CA, USA) (2) and (ii) time-lapse microscopy. On the one hand, for real-time migration assay, 100µL of a suspension with 4×10^5 cells/mL in medium without FBS were seeded onto the top of the upper chamber of a CIM-plate (Ref. 05665817001, ACEA Biosciences, Inc., San Diego, CA, USA), sealed at the bottom with a microporous polyethylene terephthalate (PET) membrane with a median pore size of 8µm, and with a lower chamber that serves as a reservoir for chemoattractant media (media with 10% FBS). Wells were previously coated in both sides during 30 min with collagen IV solution (Ref. C7521, Sigma-Aldrich, St. Louis, MO, USA) (25.5µg/cm^2). Cell migration was continuously monitored throughout the experiments by measuring changes in electrical impedance at the electrode/cell interface, as a population of cells migrated from the top to the bottom chamber. Continuous values were represented as cell index (CI), a dimensionless parameter reflecting a relative change in measured electrical impedance and quantified as a slope (*per* hour) of the first 8h. On the other hand, for time-lapse microscopy, cells seeded directly or on top of thick layers of collagen I in glass bottom MW-6 culture plates (Ref. P06G-1.5-20-F, MatTek, Ashland, MA, USA) were imaged using an automated stage in a Zeiss AxioObserver Z1

widefield microscope with temperature incubation and CO_2 control using EC Plan Neofluar 20x0.5 NA DIC objective lens. Acquisition software was ZEN 2012 (Blue Edition) (Carl Zeiss Microscopy GmbH, Göttingen, Germany). 72h videos were analysed with ImageJ software.

10. Immunohistochemistry and histology analyses.

Paraffin-embedded tissues from human HCC patients were cut into 4μm-thick sections. Primary antibodies (EGFR, TGF-β and phospho-Smad2) were incubated overnight at 4ºC and binding was developed with the Vectastain ABC kit rabbit or mouse (PK-4001 and PK-4002, Vector Laboratories Inc., Burlingame, CA, USA). Tissues were visualized in a Nikon eclipse 80i microscope with the appropriate filters. Representative images were taken with a Nikon DS-Ri1 digital camera.

Specifically for pMLC2 staining, tissue samples were subjected to deparaffinization, rehydration and heat-induced epitope retrieval using a Biocare Decloaking Chamber™ (DC2012) at 110°C for 6 min in Access Super Menarini Buffer (MP-606-PG1). Then endogenous peroxidase and phosphatase alkaline were blocked with Dual Endogenous Enzyme-Blocking Reagent (Dako, Agilent) for 10 min. Incubation with primary antibody was performed overnight at 4°C in a humidified slide chamber. Secondary antibody IgG AP (Alkaline Phosphatase) (1:100, anti-rabbit, Dako) was incubated for 1h at room temperature. Subsequently, samples were developed by incubation in Permanent Red chromogen solutions (Dako, Agilent).

11. Image analysis from IHC staining.

Whole sections from 6 different patients, stained for EGFR, TGF-β and pMLC2 were scanned using NanoZoomer S210 slide scanner (Hamamatsu, Japan). Staining quantification was performed with QuPath 0.1.2 (3) software (Centre for Cancer Research & Cell Biology, Queen's University Belfast, UK). The region of interest (ROI) was defined as viable tumour tissue excluding necrosis. Positive cell detection was

performed and three different thresholds were applied according to intensity scores (0, 1, 2 and 3). Next, software was trained creating using random trees classification algorithm combined with the intensity information, in order to differentiate tumour from stroma and immune cells.

12. Analysis of gene expression from The Cancer Genome Atlas (TCGA) database.

From TCGA database (http://cancergenome.nih.gov/), we extracted gene expression data of 327 HCC patients to analyse *EGFR*, *TGFB1*, *RHOC* and *CDC42* expression in HCC outcome. Only patients whose tumour sample contained <30% of stroma were selected to avoid interference, as some markers can be also expressed in surrounding non-tumour tissue. Normalized mRNA expression data from GISTIC were downloaded from cBioportal (4,5) and analysed as described in the "Statistical analyses" section.

13. Ethics statement.

Human HCC tissues were obtained from Pathological Anatomy Service, University Hospital of Bellvitge, Barcelona. Human tissues were collected with the required approvals from the Institutional Review Board (Ethical Committee of Clinical Research from University Hospital of Bellvitge) and patients' written consent conformed to ethical guidelines of 1975 Declaration of Helsinki.

14. References

1. Crosas-Molist E, Bertran E, Sancho P, López-Luque J, Fernando J, Sánchez A, et al. The NADPH oxidase NOX4 inhibits hepatocyte proliferation and liver cancer progression. Free Radic Biol Med. 2014;69:338–47.

2. Crosas-Molist E, Bertran E, Rodriguez-Hernandez I, Herraiz C, Cantelli G, Fabra À, et al. The NADPH oxidase NOX4 represses epithelial to amoeboid transition and efficient tumour dissemination. Oncogene. 2017;36(21):3002–14.

3. Bankhead P, Loughrey MB, Fernández JA, Dombrowski Y, McArt DG, Dunne PD, et al.

QuPath: Open source software for digital pathology image analysis. Sci Rep. 2017;7(1):16878.

4. Gao J, Aksoy BA, Dogrusoz U, Dresdner G, Gross B, Sumer SO, et al. Integrative analysis of complex cancer genomics and clinical profiles using the cBioPortal. Sci Signal. 2013;6(269):pl1.

5. Cerami E, Gao J, Dogrusoz U, Gross BE, Sumer SO, Aksoy BA, et al. The cBio cancer genomics portal: an open platform for exploring multidimensional cancer genomics data. Cancer Discov. 2012;2(5):401–4.

SUPPLEMENTARY TABLES AND FIGURES

Supplementary Table I. shRNA sequences used in this study for targeting knock-down EGFR.

shRNA (gene)	Plasmid number	Sequence (5'–3')
Control unspecific shRNA (sh-)	-	CCGGCAACAAGATGAAGAGCACCAACTCGAGTTGGTGCTCTTCATCTTGTTGTTTTT
Human EGFR (shEGFR)	#1	CCGGGTGGCTGGTTATGTCCTCATTCTCGAGAATGAGGACATAACCAGCCACTTTTTG
	#2	CCGGGCTGCTCTGAAATCTCCTTTACTCGAGTAAAGGAGATTTCAGAGCAGCTTTTTG

Supplementary Table II. Human primers sequences used in LightCycler 480 SYBR Green System quantitative PCR.

Gene	Forward (5'–3')	Reverse (5'–3')
CDC42	CAGGGCAAGAGGATTATGACAG	GTTATCTCAGGCACCCACTT
CDH1	CCCAATACATCTCCCTTCACAG	CCACCTCTAAGGCCATCTTTG
CDH2	CCCAAGACAAAGAGACCCAG	GCCACTGTGCTTACTGAATTG
EGFR	AGATCATTTTCTCAGCCTCCAG	GACATAACCAGCCACCTCC
RHOA	AGCTGGGCAGGAAGATTATG	CGTTGGGACAGAAATGCTTG
RHOC	CAAGACGAGCACACCAGG	AGCACTCAAGGTAGCCAAAG
RPL32	AACGTCAAGGAGCTGGAAG	GGGTTGGTGACTCTGATGG
SFRS4	TGGAACTGAAGTCAATGGGAG	CTGCTCTTACGGGAATGTCTG
SNAI1	GCTGCAGGACTCTAATCCAGAGTT	GACAGAGTCCCAGATGAGCATTG
SNAI2	ACACATTAGAACTCACACGGG	TGGAGAAGGTTTTGGAGCAG
TGFB1	AAGTGGACATCAACGGGTTC	GTCCTTGCGGAAGTCAATGT
TWIST1	CTCAGCTACGCCTTCTCG	ACTGTCCATTTTCTCCTTCTCTG
VIM	GGAAGCCTAACTACAGCGAG	CAGAGTCCCAGATGAGCATTG
ZEB1	ACCCTTGAAAGTGATCCAGC	CATTCCATTTTCTGTCTTCCGC
ZEB2	AGGCATATGGTGACGCACAA	CTTGAACTTGCGGTTACCTGC

Supplementary Table III. Antibodies used for immunohistochemistry, western blotting and immunofluorescence assays.

Primary antibody	Reference and purchased from	Application (working dilution)
Mouse anti β-actin (Clone AC-15)	A5441 (Sigma-Aldrich)	WB (1:5000)
Mouse anti-β-catenin	610154 (BD-Transduction)	IF (1:100)
Mouse anti-cytokeratin18	61028 (Progen Biotecknik)	IF (1:100)
Mouse anti-E-cadherin	C20820 (BD-Transduction)	IF (1:50)
Rabbit anti-EGFR	#2232 (Cell Signaling Technology)	WB (1:1000)
Rabbit anti-EGFR (D38B1) XP	#4267 (Cell Signaling Technology)	IHC (1:50)
Phalloidin-TRITC	P1951 (Sigma-Aldrich)	IF (1:500)
Rabbit anti-phospho-EGFR (Tyr1068) (D7A5) XP	#3777 (Cell Signaling Technology)	WB (1:1000)
Rabbit anti-phospho-Myosin Light Chain 2 (Ser19)	#3671 (Cell Signaling Technology)	IF (1:200) IHC (1:50)
Rabbit anti-TGFβ1 (V)	sc-146 (Santa Cruz Biotechnology)	IHC (1:50)
Rabbit anti-phospho Smad2 (Ser465/467)	#3101 (Cell Signaling Technology)	IHC (1:50)
Mouse anti-Vimentin	V6630 (Sigma-Aldrich)	IF (1:100)
Mouse anti-Vinculin	V9131 (Sigma-Aldrich)	IF (1:100)
Rabbit anti-ZO-1	61-7300 (Invitrogen)	IF (1:50)

Abbreviations: WB, Western Blotting; IF, immunofluorescence; IHC, immunohistochemistry.

<u>Supplementary Table IV.</u> Clinico-pathological characteristics of HCC patients used in this study.

Case	Aetiology	Age (years) / Gender	Size (cm)	Tumoral focus	Satellite nodules	Histological grade	Microscopic vascular invasion	Macroscopic vascular invasion	Pathologic T stage
1	ALC	46/M	3	1/0	-	3	0	0	1/I
2	ALC, HCV	50/M	2.5	2/0	-	2-3	0	0	2/II
3	ALC	75/M	3	1/0	-	3	0	0	1/I
4	U	49/F	27	1/0	-	3	0	0	1/I
5	U	78/F	7.5	1/1	1	3	1	0	2/II
6	ALC	50/M	2	9/0	-	2	1	0	2/II
7	HCV	69/M	3	-	-	3	0	1	1/I
8	HCV	61/M	2.5	-	-	2	0	0	2/II
9	U	74/M	6	1/0	-	2	0	0	1/I
10	HCV	52/M	3.8	1/0	-	2	0	0	1/I
11	U	82/M	7	1/0	-	1-2	0	0	1/I
12	HCV	46/M	8.5	1/multi	Multi	3	1	0	2/II
13	U	71/M	20	1/multi	Multi	2	1	0	2/II
14	HCV	64/M	3.3	1/0	-	3	0	0	1/I
15	HCV	71/M	4.5	1/1	1	2-3	0	0	1/I
16	U	66/M	3	1	-	2	1	0	2
17	HBV	64/M	2.9	1	-	2	0	0	1
18	HBV	58/F	2.8	1	-	2	0	0	1
19	ALC	64/M	3.2	1	-	2-3	1	0	2
20	HCV	48/M	5.5	1	-	3	1	0	3
21	HCV	69/F	3.5	1	-	3	0	0	1
22	HCV	69/M	3.5	1	-	2-3	0	0	1
23	HCV	59/M	1.8	1	-	2	0	0	1
24	U	57/F	6.5	1	-	2	0	0	1
25	U	47/M	20	1	-	1	0	0	1
26	U	47/M	2	1	-	1	0	0	1
27	ALC	58/D	2	1	-	2	0	0	2
28	HCV	68/M	2.5	1	-	2	1	0	2
29	HBV	53/M	9	1	-	3	1	0	2
30	HCV, HBV	53/M	5	1	-	3	1	0	2
31	ALC	64/M	1	1	-	2	1	0	2
32	ALC	63/M	4.2	1	-	3	1	0	2
33	U	44/M	8.3	1	-	3	1	0	2
34	HBV	67/M	5.5	4	-	3	1	0	3
35	HCV	48/M	5.5	1	-	3	1	0	2
36	HCV	68/M	2	1	-		1	No data	2
37	ALC	73/M	1.4	1	-	2	0	0	1

38	HCV	74/M	3.2	1	-	No data	0	0	1
39	HCV	49/M	9.5	1	-	2	1	0	2
40	HBV	No data	4.9	1	-	2	0	0	1
41	HCV	62/M	2.3	1	-	2	0	0	1
42	ALC	65/M	2.5	1	-	2	0	0	1
43	HCV	67/F	2.9	1	-	2	1	1	2
44	ALC	70/M	4.8	1	-	4	1	1	4
45	LC	62/M	1.9	1	-	2	0	0	1
46	LC	78/M	1.2	1	-	2	1	0	2
47	HCV	74/M	4.7	1	-	2	0	0	1
48									
49	LC	34/F	2.8	1	-	2	0	0	1
50	LC	77/M	26	1	-	2	1	0	2
51	U	64/M	8	1	-	3	1	0	2
52	HCV	76/M	4.5	1	-	2	0	0	1
53	LC	71/F	3.8	1	-	3	0	0	1
54	HCV	60/M	2.5	1	-	2	1	0	2
55	LC	66/M	1.2	1	-	3	0	0	
56	U	68/M	4	1	-	2	1	0	2
57	HCV	46/M	1.8	1	-	1	0	0	1
58	U	77/M	7	1	-	2	0	0	1
59	HCV	58/M	6.5	1	-	2	1	0	2
60	HBV	47/F	4.9	1	-	4	1	0	2
61	LC	66/M	16	1	-	2	1	0	2
62	U	79/M	4.5	1	-	3	1	0	2
63	HCV	51/M	5.8	2	-	3	1	0	3
64									

Abbreviations: Gender: F, female; M, male. Histological grade according to the criteria of Edmondson and Steiner: 1, well differentiated; 2, moderately differentiated; 3, poorly differentiated; 4, undifferentiated. Aetiology: HBV, hepatitis B virus; HCV, hepatitis C virus; ALC, heavy alcohol use; U, unknown aetiology; background: LC, liver cirrhosis.

<u>Supplementary Table V.</u> Molecular characteristics of the human HCC cell lines used in this study. Characteristics of PLC/PRF/5 and Hep3B cells.

Cell line	Tumour type	Differentiation grade	TP53 status	Other characteristics
PLC/PRF/5	Human Liver Hepatocarcinoma	Well-differentiated	Mutated p.R249S	Express ABL1, FES, MYC, HaRAS and PDGFB oncogenes
Hep3B	Human Negroid Hepatocarcinoma	Well-differentiated	Deleted	Deficient in functional RB1; FAS mutations

Abbreviations: ABL1, Abelson murine leukemia viral oncogene homolog 1; FES, feline sarcoma oncogene; MYC, myc protooncogene; PDGFB, platelet derived growth factor subunit B; RB1, retinoblasmtoma; FAS, Fas cell surface death receptor.

<u>Supplementary Table VI.</u> Correlation of *EGFR*, *TGFB1* and *RHOC* expressions with the HCC tumour grade (G1/G2 or G3/G4), analysed from TCGA database.

	Tumour Grade	**G1/G2**	**G3/G4**
High *EGFR* and High *TGFB1*	Count (%)	39 (69.6)	17 (30.4)
Low *EGFR* and High *TGFB1*	Count (%)	36 (54.5)	30 (45.5)
High *EGFR* and High *RHOC*	Count (%)	40 (78.4)	11 (21.6)
Low *EGFR* and High *RHOC*	Count (%)	43 (60.6)	28 (39.4)

Abbreviations: G1/G2, well differentiated/moderately differentiated (low grade); G3/G4, poorly differentiated/undifferentiated (high grade).

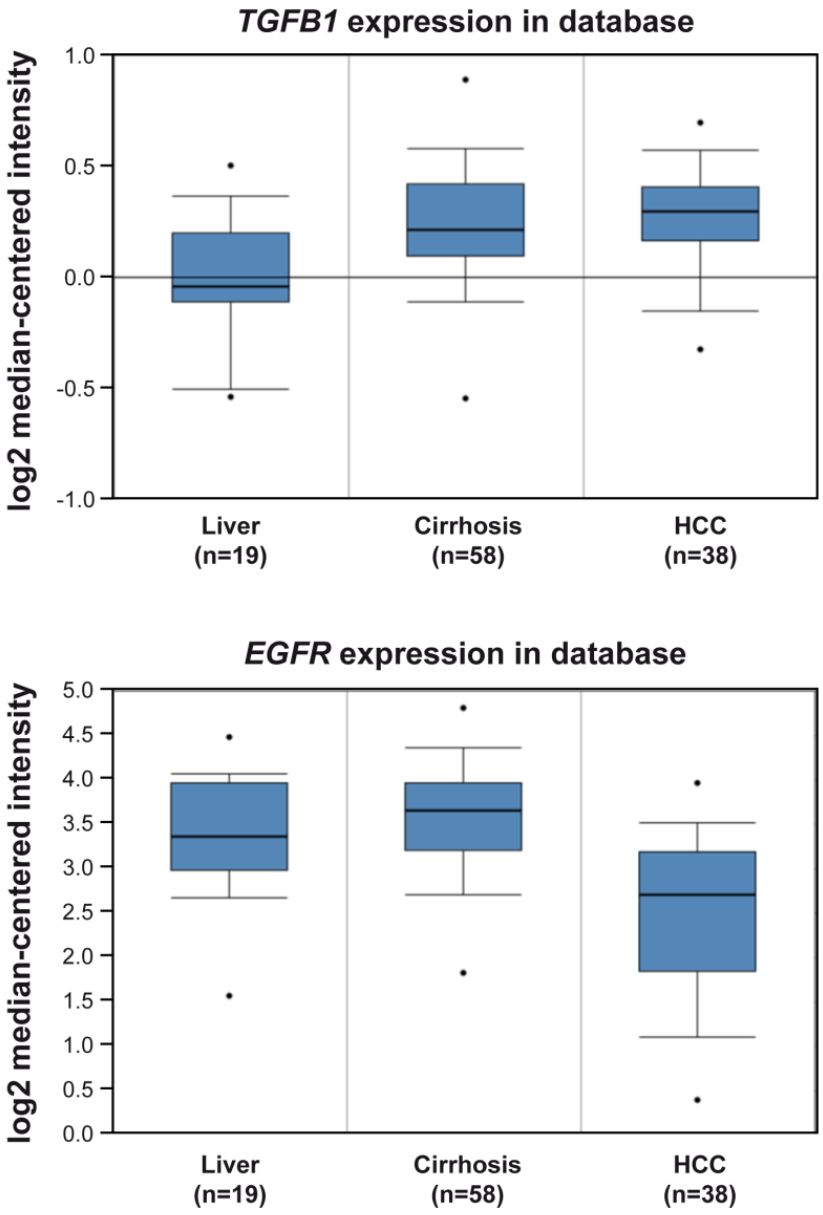

Supplementary Figure S1. Analysis of *EGFR* and *TGFB1* expression in databases. *TGFB1* and EGFR mRNA expression in the Mas Liver database from Oncomine (N=115).

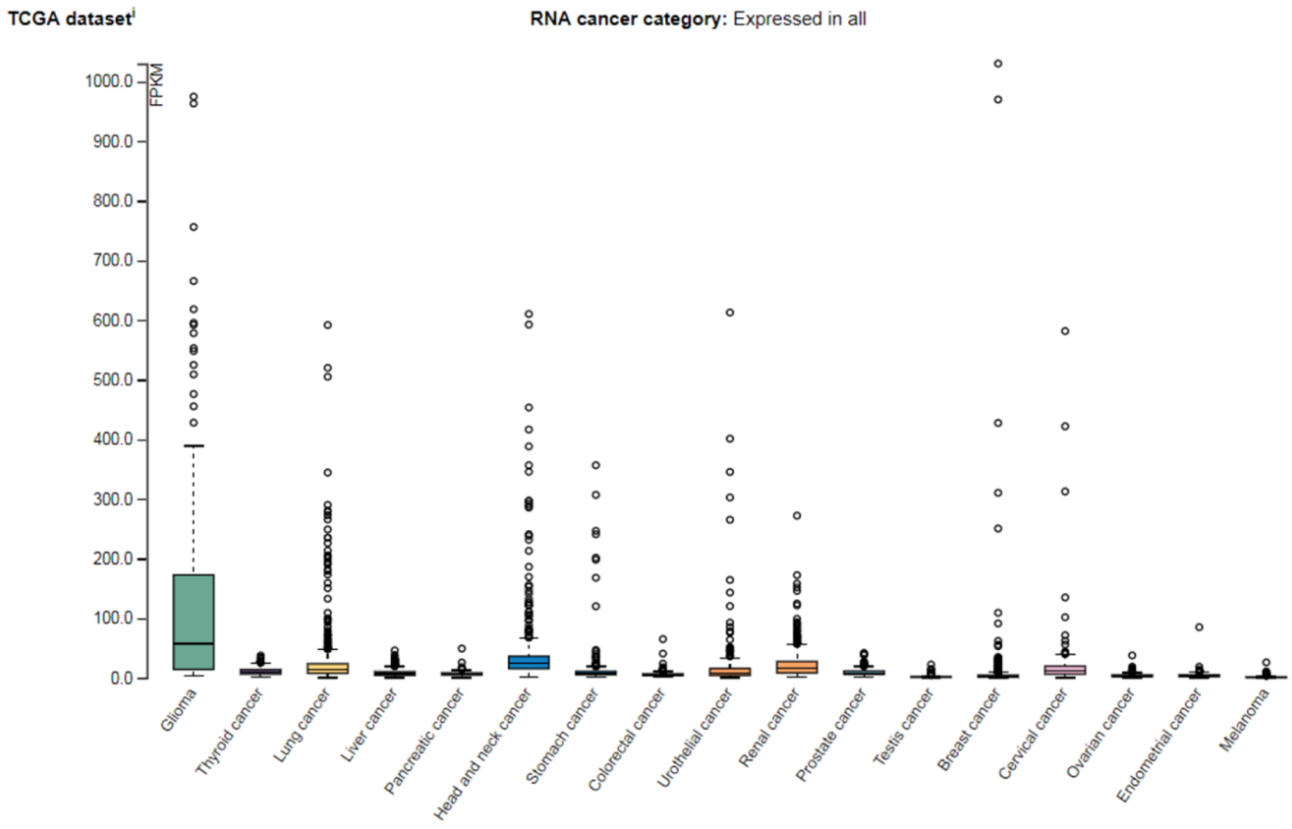

Supplementary Figure S2. Human Protein Atlas and TCGA dataset for pan-cancer RNA expression of *EGFR*.

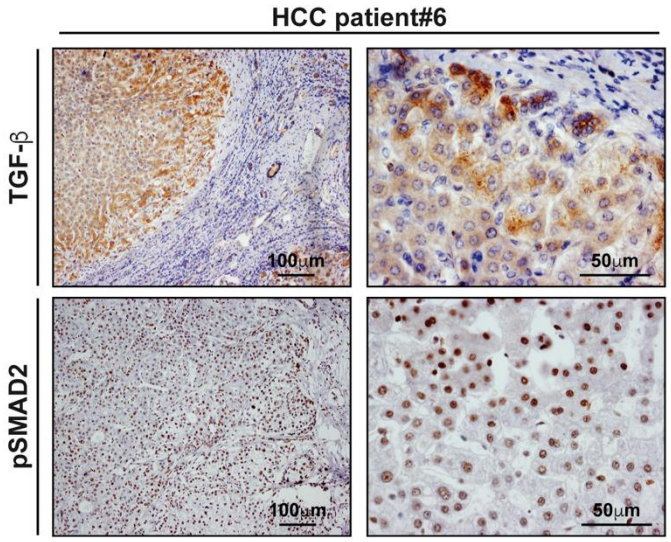

Supplementary Figure S3. Most HCC patients presented a high TGF-β expression concomitant with a higher SMAD2 phosphorylation. Immunohistochemistry of TGF-β and pSMAD2 in tissues from the cohort of HCC patients. Representative 10x and 40x images are shown.

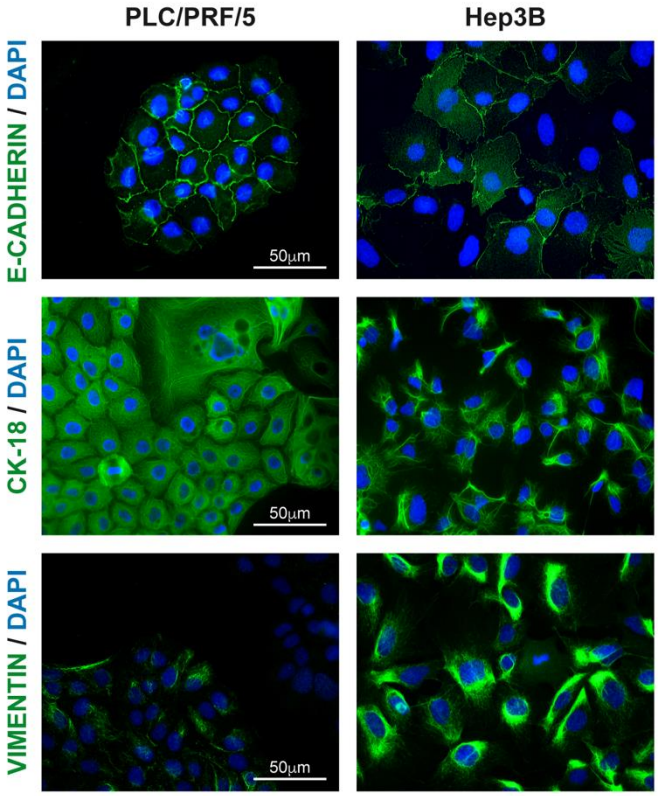

Supplementary Figure S4. Phenotypical characterization of PLC/PRF/5 and Hep3B HCC cell lines. Immunostaining of E-CADHERIN, CK-18 and VIMENTIN (green), and DAPI (blue: nuclei) in PLC/PRF/5 and Hep3B cells cultured under basal conditions (10% FBS). Representative 40x images are shown.

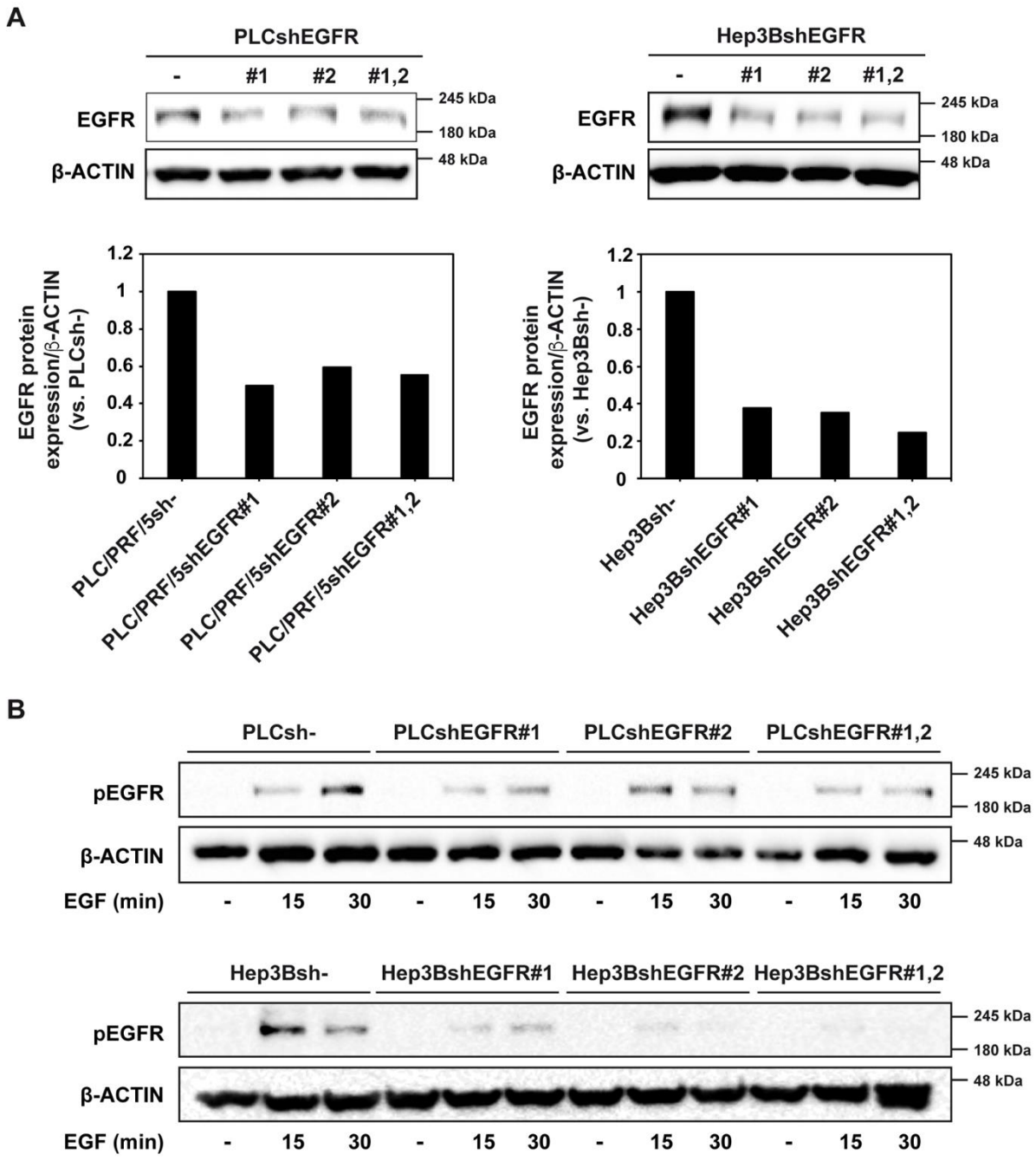

Supplementary Figure S5. Western blot analysis to confirm EGFR stable silencing in PLC/PRF/5 and Hep3B cells. PLC/PRF/5 and Hep3B cells were stably transfected either with an unspecific CONTROL shRNA (sh-) or with different plasmids against EGFR. Independent clones (#1 or #2) and pooled cell populations (#1,2) are shown. **A)** Analysis of EGFR protein levels by Western blot of the different clones **(upper)** and the corresponding densitometric analysis **(lower)**. **B)** Western blot analysis of the response to EGF treatment (20ng/mL) in terms of EGFR phosphorylation in both HCC cell lines. β-ACTIN was used as loading control.

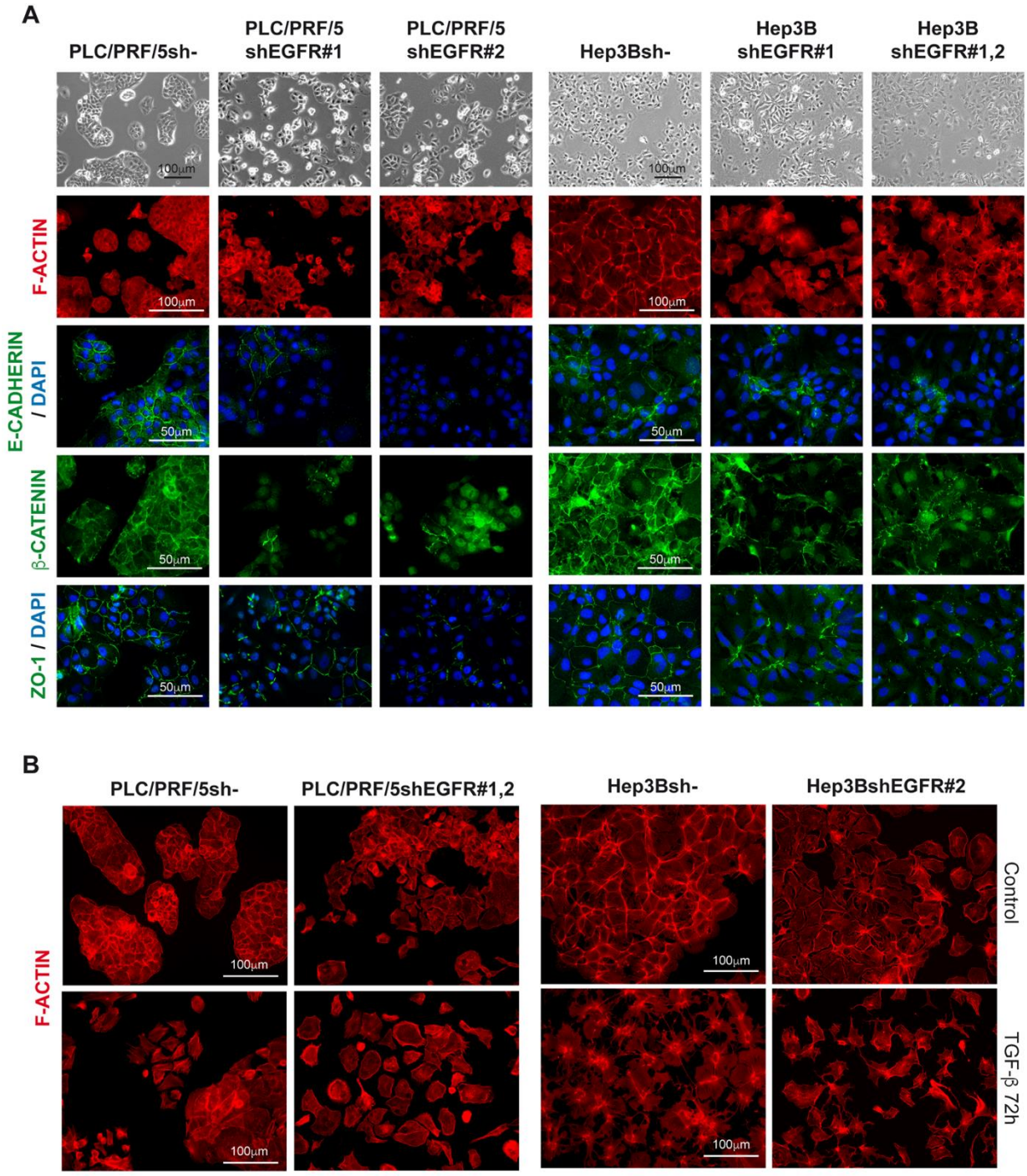

Supplementary Figure S6 (complements Fig. 2). Effect of EGFR silencing on cell-cell contacts in HCC cells. Unsilenced and EGFR silenced PLC/PRF/5 and Hep3B cells cultured on plastic. **A)** Phase contrast microscopy photographs, and immunostaining of F-ACTIN (red), E-CADHERIN, β-CATENIN and ZO-1 (green), and DAPI (blue: nuclei) of two more different clones. **B)** Immunostaining of F-ACTIN (red) in both unsilenced and EGFR silenced HCC cells after TGF-β treatment (2ng/mL) for 72h. Representative 20x and 40x images are shown.

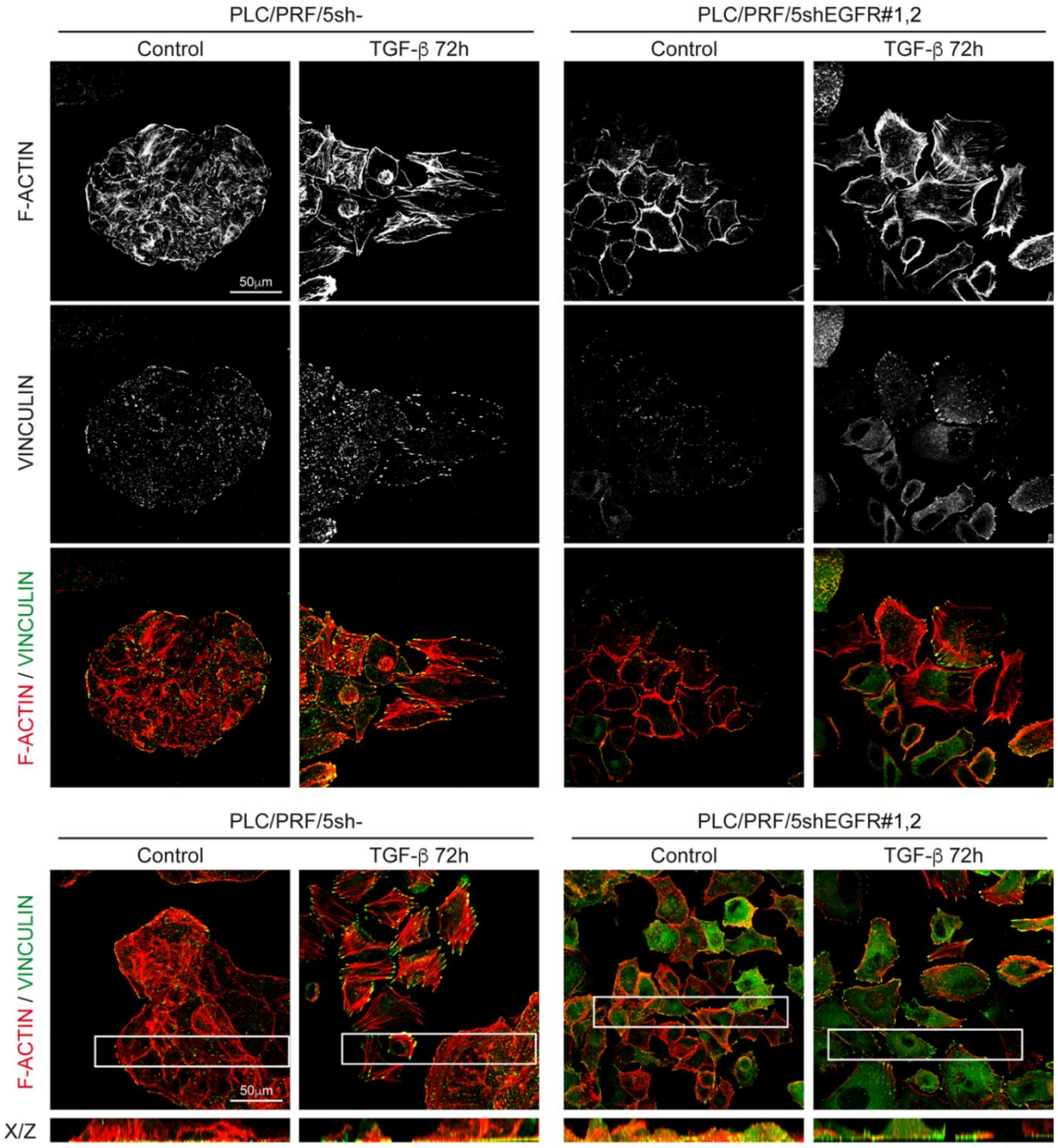

Supplementary Figure S7 (complements Fig. 3). Effect of EGFR silencing on cell-to-matrix adhesion in terms of focal adhesions in HCC cells, untreated or treated with TGF-β. Immunostaining of VINCULIN (green) and F-ACTIN (red) after TGF-β treatment (2ng/mL) for 72h in unsilenced and EGFR silenced PLC/PRF/5 cells cultured on plastic. Representative 40x confocal images of one stack from the cells' bottom **(upper panel)** and all the stacks from the cells (0.25μm thick/stack) **(lower panel)** are shown. A detail of the X/Z axis is shown at the bottom of these images.

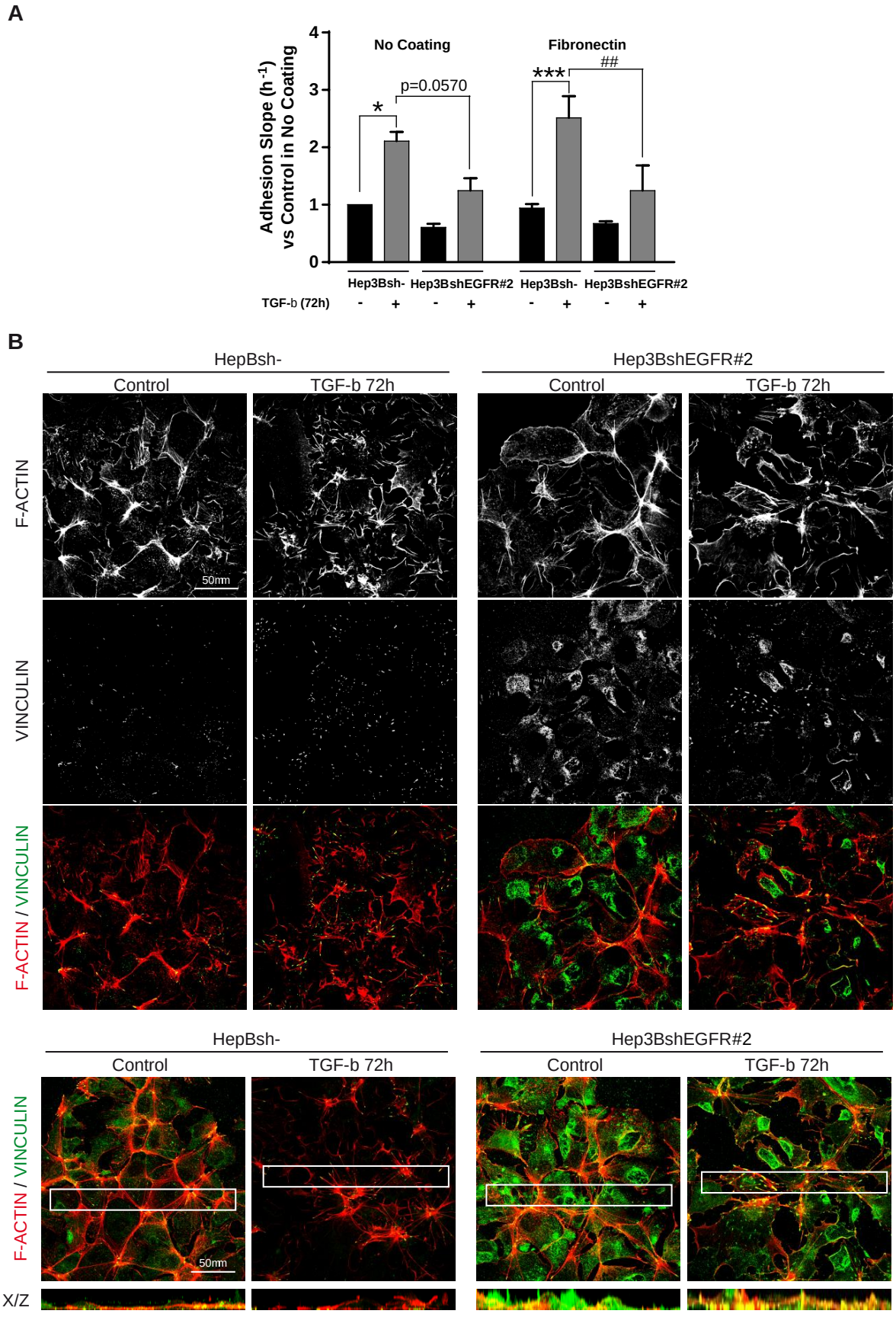

(Figure legend in the next page)

Supplementary Figure S8. Effect of EGFR silencing on cell-to-matrix adhesion in HCC cells, untreated or treated with TGF-β. A) Unsilenced and EGFR silenced Hep3B cells were treated with TGF-β (2ng/mL) during 68h, then trypsinized and plated in the xCELLigence system for a real-time adhesion assay. Adhesion was then assessed during 4h, and it is expressed as relative to Hep3B unsilenced and untreated cells in no coating and fibronectin coating conditions. Data are mean ± SEM of 3 independent experiments performed in biological duplicates. Two-way ANOVA was used: *$p<0.05$ and ***$p<0.001$ compared to control untreated cells in each cell line (unsilenced or silenced); ##$p<0.01$ compared to unsilenced cells in each condition (untreated or treated). **B)** Immunostaining of VINCULIN (green) and F-ACTIN (red) after TGF-β treatment (2ng/mL) for 72h in unsilenced and EGFR silenced Hep3B cells cultured on plastic. Representative 40x confocal images of one stack from the cells' bottom **(upper)** and all the stacks from the cells (0.25μm thick/stack) **(lower)** are shown. A detail of the X/Z axis is shown at the bottom of these images.

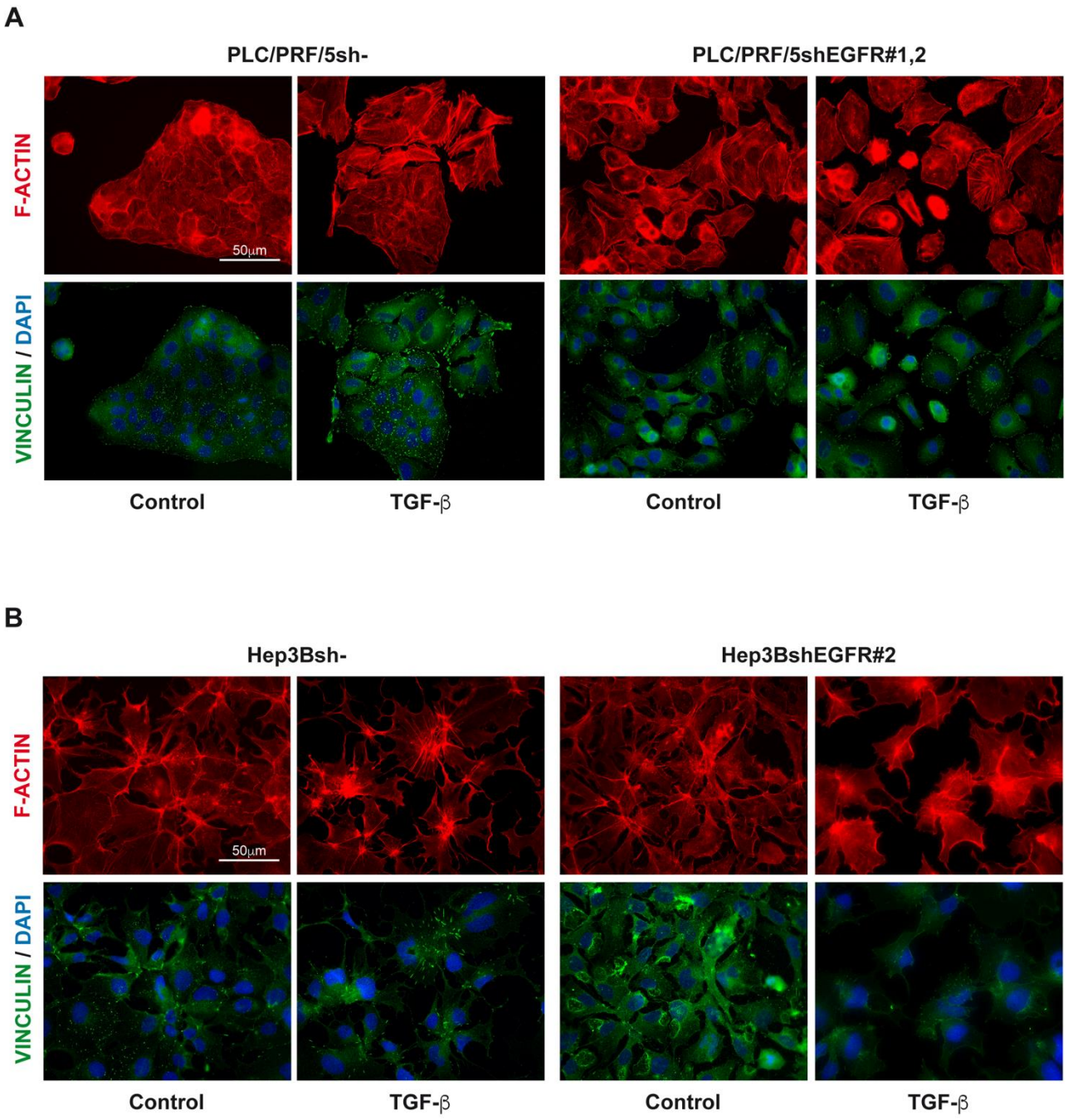

Supplementary Figure S9. Effect of EGFR silencing on cell-to-matrix adhesion in terms of focal adhesions in HCC cells, untreated or treated with TGF-β, cultured on Fibronectin. Immunostaining of VINCULIN (green) and F-ACTIN (red) after TGF-β treatment (2ng/mL) for 72h in unsilenced and EGFR silenced PLC/PRF/5 **(A)** and Hep3B **(B)** cells cultured on top of fibronectin coated glass coverslips. Representative 40x epifluorescence images are shown.

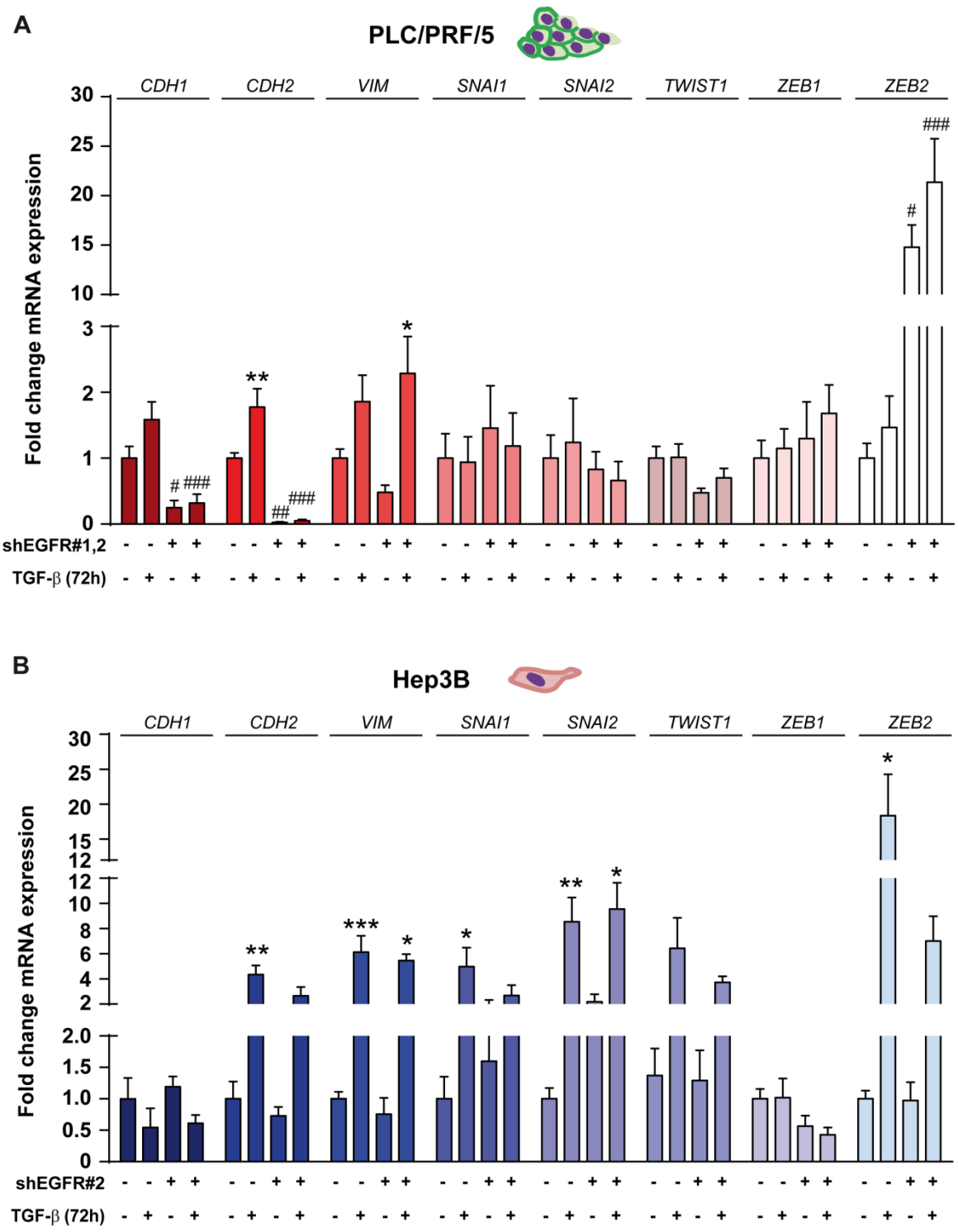

(Figure legend in the next page)

Supplementary Figure S10. Role of the EGFR pathway in the TGF-β-induced modulation of the EMT phenotype in HCC cells. qRT-PCR analysis of E-CADHERIN (*CDH1*), N-CADHERIN (*CDH2*), VIMENTIN (*VIM*), SNAIL (*SNAI1*), SLUG (*SNAI2*), TWIST (*TWIST1*), ZEB1 (*ZEB1*) and ZEB2 (*ZEB2*) mRNA levels in EGFR silenced PLC/PRF/5 **(A)** and Hep3B **(B)** cells after 72h of TGF-β treatment (2ng/mL). Data in A and B are mean ± SEM of ≥3 independent experiments. Two-way ANOVA was used: *p<0.05, **p<0.01 and ***p<0.001 compared to control untreated cells in each cell line (unsilenced or silenced); #p<0.05, ##p<0.01 and ###p<0.001 compared to unsilenced cells in each condition (untreated or treated).

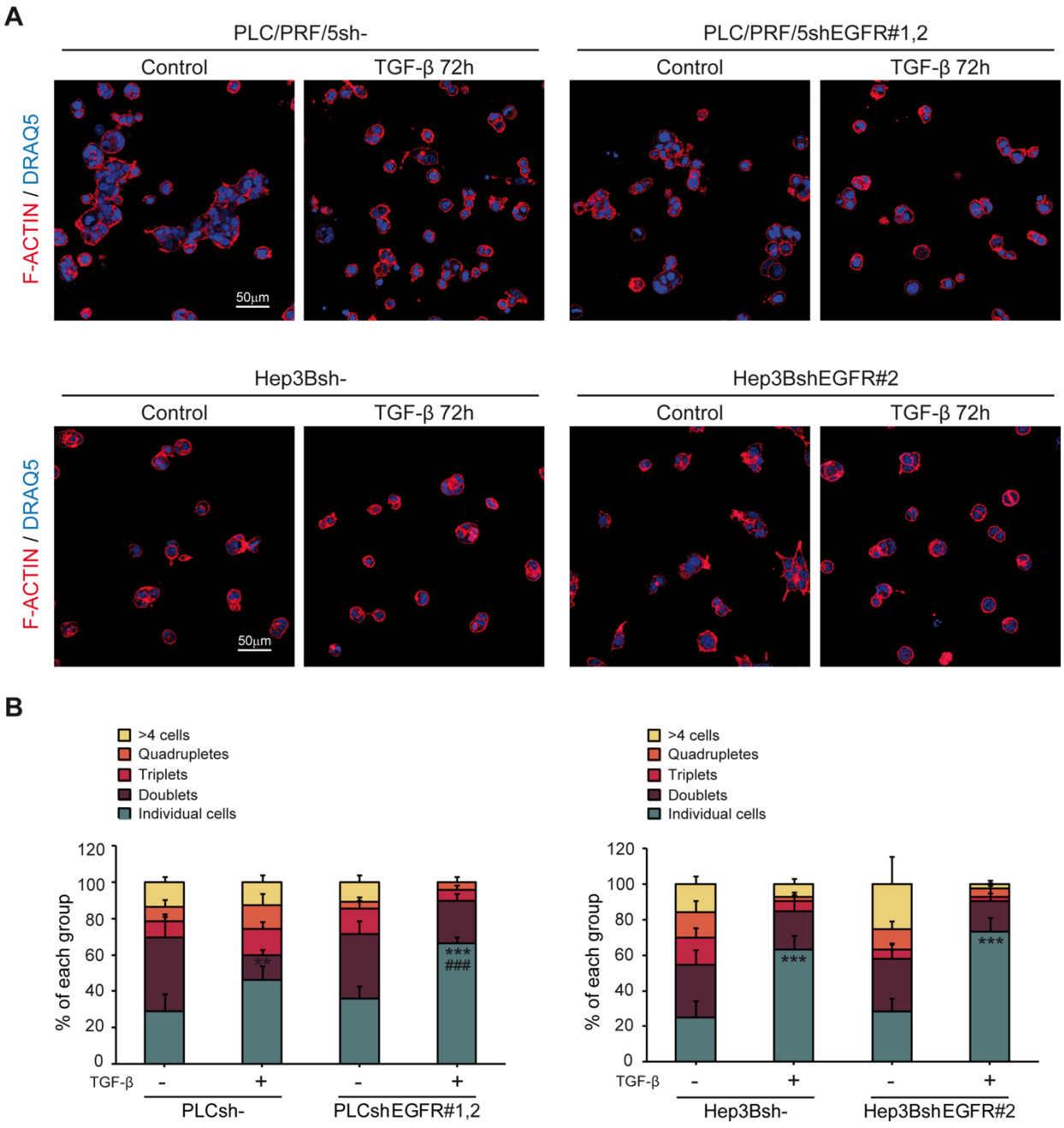

(Figure legend in the next page)

Supplementary Figure S11. EGFR silenced PLC/PRF/5 and Hep3B cells cultured on top of a matrix of collagen I. Unsilenced and EGFR silenced PLC/PRF/5 and Hep3B cells were cultured on plastic and treated with TGF-β (2ng/mL) during 48h. Then, cells were trypsinized and cultured on top of a bovine collagen I matrix for 24h more, up to a total of 72h with TGF-β treatment. Representative 40x confocal images of one stack of immunostaining of F-ACTIN (red) and DRAQ5 (blue: nuclei) of PLC/PRF/5 and Hep3B cells are shown. **B)** Quantification of the number of cells *per* group in PLC/PRF/5 and Hep3B cells. Data are mean ± SEM of 3 independent experiments performed in duplicates, and ≥5 fields *per* condition were quantified. Two-way ANOVA was used: **p<0.01 and ***p<0.001 compared to control untreated cells in each cell line (unsilenced or silenced); ###p<0.001 compared to unsilenced cells in each condition (untreated or treated).

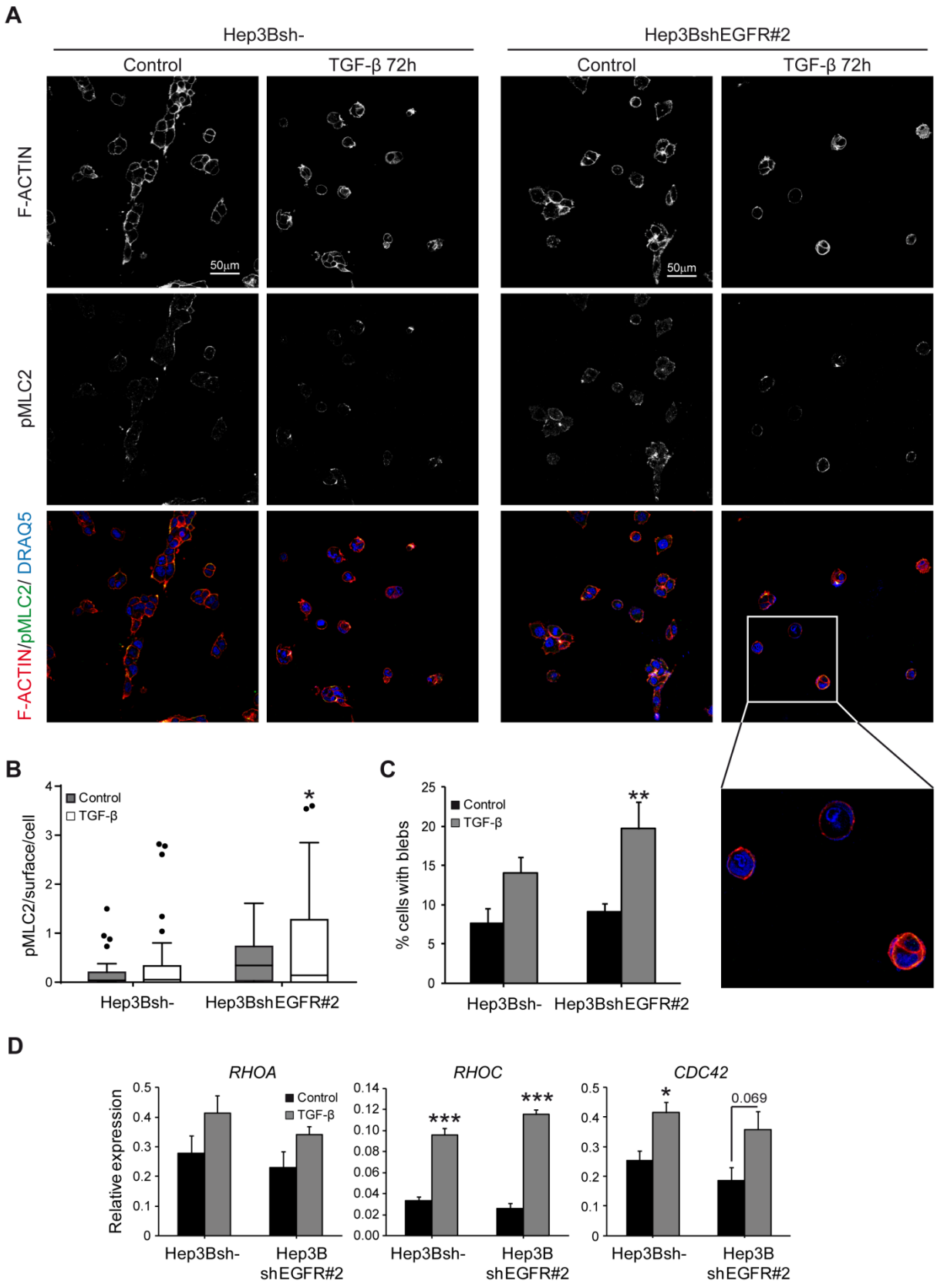

(Figure legend in the next page)

Supplementary Figure S12. Effect of EGFR silencing on actomyosin contractility in HCC cells after TGF-β treatment when cultured on top of a matrix of collagen I. Unsilenced and EGFR silenced Hep3B cells were cultured on plastic and treated with TGF-β (2ng/mL) during 48h. Cells were then trypsinized and cultured on top of a bovine collagen I matrix for 24h more, up to a total of 72h with TGF-β treatment. **A)** Representative 40x confocal images of one stack of immunostaining of pMLC2 (green), F-ACTIN (red), and DRAQ5 (blue: nuclei) are shown. **B)** Quantification of pMLC2 immunostaining intensity *per* surface and cell. **C)** Quantification of the percentage of cells with blebs. **D)** qRT-PCR analysis of RHOA (*RHOA*), RHOC (*RHOC*) and CDC42 (*CDC42*) mRNA levels in unsilenced and EGFR silenced Hep3B cells after 72h of TGF-β treatment (2ng/mL) when cells were cultured on plastic. Data in B and C are mean ± SEM of 3 experiment performed in duplicates and ≥5 fields *per* condition were quantified. Data in D are mean ± SEM of ≥3 independent experiments. Two-way ANOVA was used: *p<0.05, **p<0.01 and ***p<0.001 compared to control untreated cells in each cell line (unsilenced or silenced).

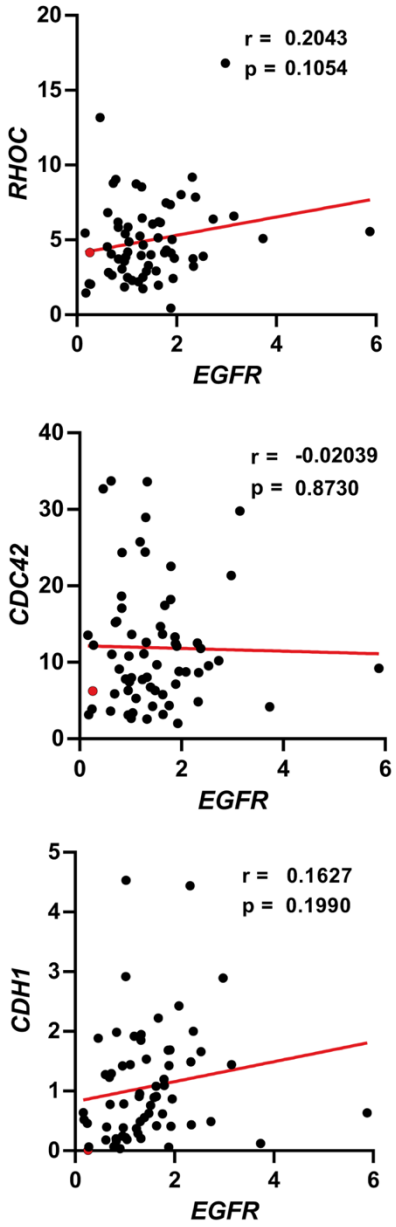

Supplementary Figure S13. Correlation between *RHOC, CDC42* and *CDH1 versus EGFR* tumour expression in HCC patients. Linear correlation analysis among mentioned genes expression analysed by qRT-PCR in the cohort of 64 samples from HCC patients. Each dot represents relative expression of each HCC tumour tissue.

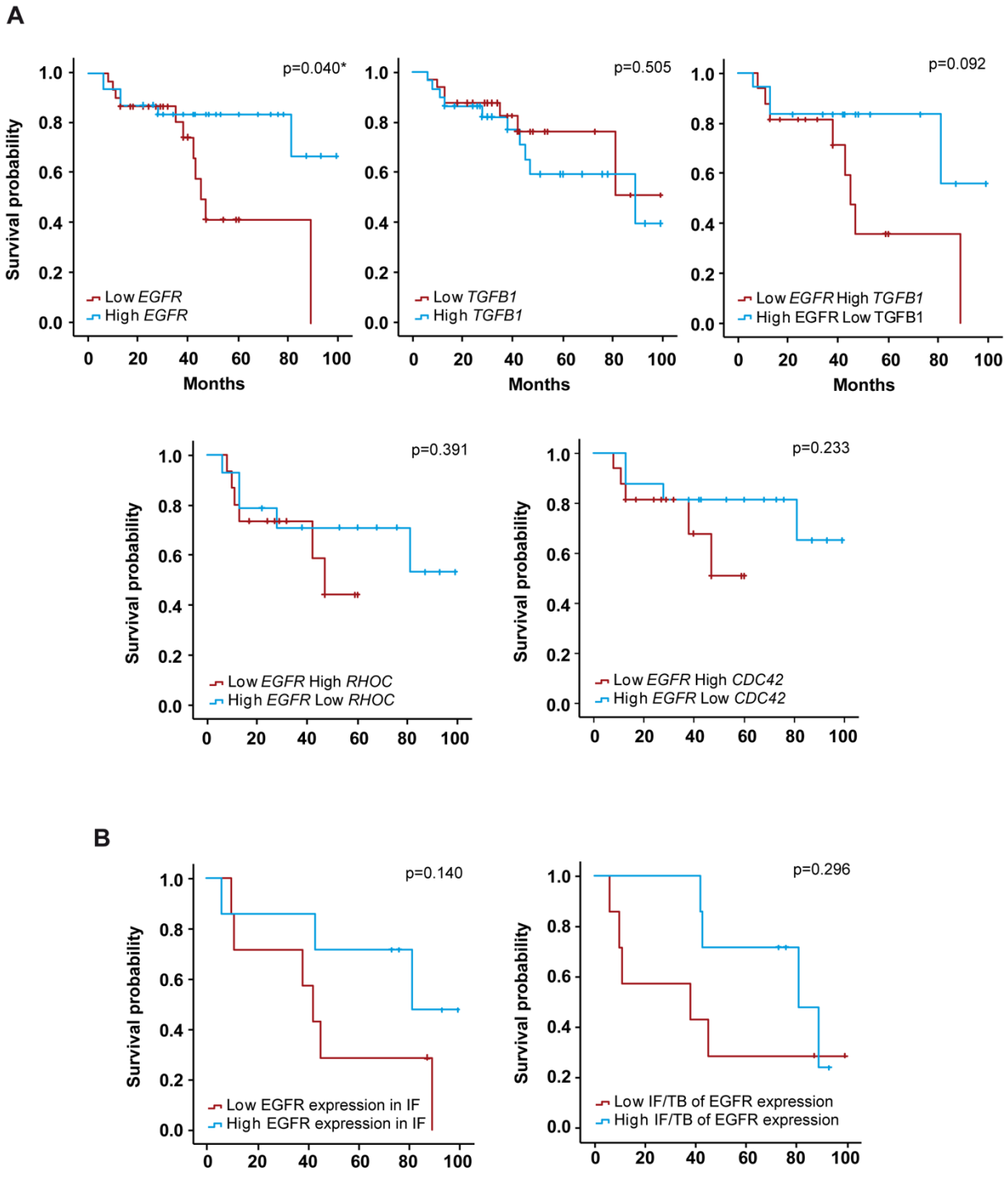

(Figure legend in the next page)

Supplementary Figure S14. Analysis of *EGFR, TGFB1* and related genes expression in tissues from HCC patients shows prognosis significance. A) Kaplan-Meier estimation of 100 months survival in the cohort of 64 HCC patients, according to *EGFR* expression, *TGFB1* expression and the combination of both, as well as according to *EGFR* expression combined with *RHOC* and *CDC42* expression (N=64 HCC patients). **B)** Kaplan-Meier estimation of 100 months survival according to EGFR expression in TB and the IF after performing a staining for EGFR in a cohort of 16 HCC patients. Survival representation comparing high and low expression of EGFR at the invasion front **(left)** and survival representation comparing high and low IF/TB fold change of EGFR **(right)**. Cut-off median. Kaplan–Meier method using the log-rank test was used: *$p<0.05$.

Supplementary Video 1. Effect of EGFR silencing on the migration capacity in HCC cells. Migration in unsilenced PLC/PRF/5 cells (PLC/PRF/5sh-) was assessed in a 2D matrix. 36h of time-lapse video microscopy is shown.

Supplementary Video 2. Effect of EGFR silencing on the migration capacity in HCC cells. Migration in unsilenced PLC/PRF/5 cells (PLC/PRF/5sh-) upon TGF-β treatment was assessed in a 2D matrix. 36h of time-lapse video microscopy is shown.

Supplementary Video 3. Effect of EGFR silencing on the migration capacity in HCC cells. Migration in EGFR silenced PLC/PRF/5 cells (PLC/PRF/5shEGFR) was assessed in a 2D matrix. 36h of time-lapse video microscopy is shown.

Supplementary Video 4. Effect of EGFR silencing on the migration capacity in HCC cells. Migration in EGFR silenced PLC/PRF/5 cells (PLC/PRF/5shEGFR) upon TGF-β treatment was assessed in a 2D matrix. 36h of time-lapse video microscopy is shown.

Supplementary Video 5. Effect of EGFR silencing on the migration capacity in HCC cells. Migration in unsilenced Hep3B cells (Hep3Bsh-) was assessed in a 2D matrix. 36h of time-lapse video microscopy is shown.

Supplementary Video 6. Effect of EGFR silencing on the migration capacity in HCC cells. Migration in unsilenced Hep3B cells (Hep3Bsh-) upon TGF-β treatment was assessed in a 2D matrix. 36h of time-lapse video microscopy is shown.

Supplementary Video 7. Effect of EGFR silencing on the migration capacity in HCC cells. Migration in EGFR silenced Hep3B cells (Hep3BshEGFR) was assessed in a 2D matrix. 36h of time-lapse video microscopy is shown.

Supplementary Video 8. Effect of EGFR silencing on the migration capacity in HCC cells. Migration in EGFR silenced Hep3B cells (Hep3BshEGFR) upon TGF-β treatment was assessed in a 2D matrix. 36h of time-lapse video microscopy is shown.

Supplementary Video 9. Effect of EGFR silencing on the migration capacity in HCC cells. Migration in unsilenced PLC/PRF/5 cells (PLC/PRF/5sh-) was assessed in a 3D matrix. 20h of time-lapse video microscopy is shown.

Supplementary Video 10. Effect of EGFR silencing on the migration capacity in HCC cells. Migration in unsilenced PLC/PRF/5 cells (PLC/PRF/5sh-) upon TGF-β treatment was assessed in a 3D matrix. 16h of time-lapse video microscopy is shown.

Supplementary Video 11. Effect of EGFR silencing on the migration capacity in HCC cells. Migration in EGFR silenced PLC/PRF/5 cells (PLC/PRF/5shEGFR) was assessed in a 3D matrix. 20h of time-lapse video microscopy is shown.

Supplementary Video 12. Effect of EGFR silencing on the migration capacity in HCC cells. Migration in EGFR silenced PLC/PRF/5 cells (PLC/PRF/5shEGFR) upon TGF-β treatment was assessed in a 3D matrix. 20h of time-lapse video microscopy is shown.